Ferromagnetism Stabilized by Lattice Distortion at the Surface of the *p*-Wave Superconductor Sr$_2$RuO$_4$

R. Matzdorf,[1] Z. Fang,[3] Ismail,[1] Jiandi Zhang,[2] T. Kimura,[3] Y. Tokura,[3,4] K. Terakura,[3] E. W. Plummer[1]*

Ferromagnetic (FM) spin fluctuations are believed to mediate the spin-triplet pairing for the *p*-wave superconductivity in Sr$_2$RuO$_4$. Our experiments show that, at the surface, a bulk soft-phonon mode freezes into a static lattice distortion associated with an in-plane rotation of the RuO$_6$ octahedron. First-principle calculations confirm this structure and predict a FM ground state at the surface. This coupling between structure and magnetism in the environment of broken symmetry at the surface allows a reconsideration of the coupling mechanism in the bulk.

Sr$_2$RuO$_4$, the only known layered perovskite without copper that exhibits superconductivity (*1*), has attracted much attention because it shows spin-triplet pairing with a *p*-wave order parameter (*2*, *3*) and because the bulk has a nondistorted tetragonal K$_2$NiF$_4$ structure (*4*) with a nonmagnetic ground state. A common feature in this class of materials is that the energy difference between different structural or magnetic phases is very small, and the ground state of Sr$_2$RuO$_4$ is close to structural and magnetic instabilities. Inelastic neutron scattering experiments show that the phonon mode corresponding to the in-plane octahedron rotation with Σ_3 symmetry exhibits a large drop in energy near the zone boundary (*5*). The existence of different spin fluctuations, including FM spin fluctuations, has been documented by nuclear magnetic resonance (*6*, *7*) experiments and neutron scattering (*10*). Theory suggests that the spin-triplet pairing for the unconventional superconductivity in Sr$_2$RuO$_4$ is mediated by exchange of FM spin fluctuations (*8*). However, the recent observation of strong incommensurate spin fluctuation (*9*, *10*) indicates that more concrete evidence of FM spin fluctuation is needed. Our experiments show that the zone boundary soft phonon freezes into a static lattice distortion at the surface of Sr$_2$RuO$_4$, and our first-principle calculations predict that this lattice distortion enhances

FM fluctuations, which in turn enhances the stability of the distortion producing a FM ground state. Undoubtedly, this behavior at the surface is a direct consequence of the close coupling in the bulk between spin fluctuations and the lattice dynamics.

Single crystals were grown by the optical floating zone technique, and the two samples studied exhibited superconductivity below ~0.7 and ~1 K (*11*). Scanning tunneling microscopy (STM) images of the freshly cleaved surfaces show extremely large flat terraces with an extension of up to 10 μm by 10 μm (Fig. 1A). All step heights (Fig. 1B) are integral multiples of half the unit cell height (6.4 Å) shown in Fig. 1C. This observation ensures that we observed the surfaces of Sr$_2$RuO$_4$, not a stacking fault (or intergrowth) of a different stoichiometry such as SrRuO$_3$ or Sr$_3$Ru$_2$O$_7$.

In contrast to the bulk-like termination perpendicular to the surface, the lateral structure at the surface is clearly not the same as the bulk. At all temperatures studied with low-energy electron diffraction (LEED), $80 < T < 300$ K, we observed fractional spots corresponding to a $(\sqrt{2} \times \sqrt{2})R45°$ unit cell (Fig. 2A). Certain fractional spots were extinct at all energies, indicating that the surface unit cell has a *p*4*gm* plane group symmetry. Atomically resolved STM images (taken in the constant current mode) like the one shown in Fig. 2B exhibit the same surface unit cell $\{(\sqrt{2} \times \sqrt{2})R45°\}$ as determined by LEED (*12*). The size of these reconstructed (nearly defect-free) regions observed with the STM was appreciably larger than the coherence of the LEED beam (~100 Å by ~100 Å). The qualitative character of the image appeared to be independent of bias polarity, indicating that the image is not a result of a charge density wave. Our total

energy calculations and surface structure analysis with LEED *I-V* (intensity as a function of voltage) data show that the sample cleaves as expected between the two weakly bonded rock-salt layers without breaking the RuO$_6$ octahedra (compare with Fig. 1C).

STM does not reveal subsurface atomic information, so a quantitative analysis of the LEED beam intensity as a function of beam voltage was undertaken. The intensity versus energy of five nonequivalent integer beams (total energy range 1730 eV) and three nonequivalent fractional beams (total energy range 315 eV) was measured and compared with calculated intensities for surface model structures compatible with the *p*4*gm* symmetry. Spectra were calculated with the Barbieri/Van Hove Symmetrized Automated Tensor LEED package. The best fit (Pendry *R*-factor = 0.16) to experimental spectra was obtained for a surface structure with the octahedra rotated by $9° \pm 3°$ around the *c* axis (Fig. 2C). The static structure at the surface is the displacement pattern of the Σ_3 bulk phonon mode (*5*) at the zone boundary. The lateral displacement of the oxygen atoms in the RuO$_2$ plane due to octahedron rotation is 0.3 Å. Within the experimental error of ± 0.05 Å, the interlayer spacing at the surface is the same as in the bulk. Possible atomic displacements that would break the *p*4*gm* symmetry were estimated from the ratio of the background at the forbidden fractional order spots to the allowed fractional order spots to be <0.02 Å for Sr and Ru and <0.04 Å for oxygen, respectively. The structure analysis has been reproduced on samples from two different sources (*13*).

First-principle calculations of the ground state surface structure were conducted within the generalized gradient approximation (GGA) with the plane-wave basis pseudopotential method. Repeated slabs, which consist of three perovskite unit layers separated by a vacuum region of 12 to 14 Å, were used to simulate the surface. This calculational scheme yields bulk lattice constants within 1% (expansion) of the measured values. For the surface slab calculations, the optimized bulk lattice parameter within the *ab* plane was used. The 2*p* states of oxygen and 4*d* states of Ru were treated by the ultrasoft pseudopotential (*14*), and the cutoff energy for the wave functions expansion was 30.25 rydberg. In this layered perovskite, the thin-slab calculation is a very reliable scheme to simulate the surface of a semi-infinite system, particularly, where the *d*-band region controls the basic physics, because *d*-*d* hopping across the insulating SrO layer is virtually nonexistent. For example, the electronic structure for a slab calculation with a bulk-terminated atomic structure is, in the *d*-band region, almost identical to the bulk electronic structure.

[1]Department of Physics and Astronomy, The University of Tennessee, Knoxville, TN 37996–1200, and Oak Ridge National Laboratory (ORNL), Oak Ridge, TN 37831–6057, USA. [2]Department of Physics, Florida International University, Miami, FL 33199, USA. [3]Joint Research Center for Atom Technology (JRCAT), Tsukuba 305-0046, Japan. [4]Department of Applied Physics, University of Tokyo, Tokyo 113-0033, Japan.

*To whom correspondence should be addressed. E-mail: eplummer@utk.edu

Fig. 1. (A) STM image of a 4 μm by 4 μm surface area showing extremely large terraces and steps. **(B)** Height along the line scan shown in the STM image. **(C)** Ball model of the bulk unit cell of Sr_2RuO_4. Red, strontium; blue, oxygen; and green, ruthenium (in the center of the octahedron).
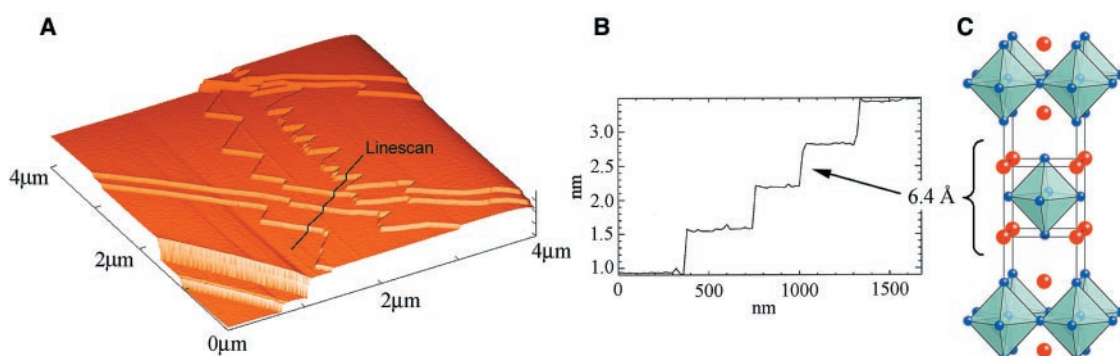
Fig. 2. (A) LEED pattern showing fractional spots (marked by arrows) according to the surface reconstruction. Fractional spots are extinct on glide lines, indicated by white lines. Electron energy $E = 195$ eV, temperature $T = 80$ K. **(B)** Atomically resolved STM image of 26 Å by 26 Å containing 7 by 7 strontium sites. Theoretical calculation of the local density of states showed that the bright spots correspond to the strontium site ($T = 300$ K and sample bias voltage = −0.75 V). The bulk (blue square) and surface unit cell (green diamond) are indicated. The image has been smoothed for clarity. **(C)** Ball model of the surface structure with rotated octahedra (top view). Orientation corresponds to the STM image (B). The direction of propagation of the bulk Σ_3 phonon mode is in the diagonal direction.
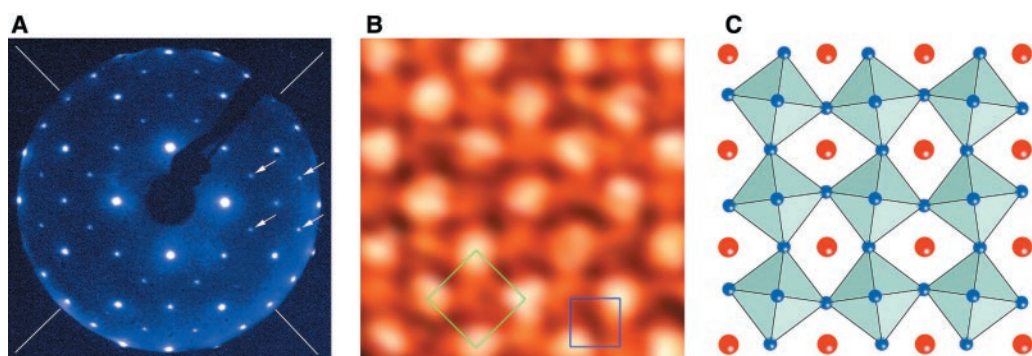
Our calculations confirm that octahedra rotation indeed happens on the surface but not in the bulk (Fig. 3). The optimized structure for a nonmagnetic surface is a surface layer with octahedra rotated by 6.5° (Fig. 3). This reconstruction, driven by compressive strain in the RuO_2 layers, lowers the energy by 14 meV per formula unit (f.u.). The FM ordering stabilizes the distortion further and increases the rotation angle to 9° (Fig. 3) to gain additional energy of 51 meV/f.u. Theoretically, the FM ground state has an exchange splitting of ~0.5 eV for Ru 4d bands at the surface and the magnetic moment on each Ru atom is 1.0 μ$_B$ (Bohr magneton).

The generalized gradient approximation (GGA) calculations slightly favor (4 meV/f.u.) a FM state for bulk (15). However, the ~50 meV/f.u. gain in energy associated with the reconstruction at the surface is very large compared with the GGA bulk FM stabilization energy. Also the surface magnetic moment of 1.0 μ$_B$/Ru is greatly enhanced, compared with the 0.4 μ$_B$/Ru value calculated (GGA) for the bulk. Our calculations shown in Fig. 3 also show that a commensurately ordered surface antiferromagnetic (AF) state with planar $\mathbf{Q} = (\pi/a, \pi/a)$ has higher energy than the FM state. There is no mechanism on the surface to stabilize the incommensurate magnetic spin fluctuation corresponding to the bulk (9, 10), located at q = (0.6pπ/a, 0.6π/a, 0), because it does not couple with the

frozen zone boundary mode of the lattice distortion. Therefore, we expect that the incommensurate spin ordering will not be more stable than the FM ordering (16–19). A cursory comparison of our FM and nonmagnetic band structure with existing photoemission data (17–19) would indicate that the surface does not have a long-range FM order at ~10 K.

The coupling between a static lattice distortion and FM order at the surface infers that the same coupling takes place in the bulk between the corresponding low-lying excitations—FM spin fluctuations and the Σ_3 soft-phonon mode that corresponds to the octahedron rotation. A very simple and straightforward picture emerges for our data and calculations by analyzing the orbital character associated with the different sheets of the Fermi surface, the Σ_3 soft phonon, and FM spin fluctuations in the bulk. There are three t_{2g} orbitals (4d_{xy}, 4d_{yz}, and 4d_{zx}) contributing to the electronic states at the Fermi energy (E_F). Here, the key orbital is the d_{xy} because the Σ_3 bulk-phonon mode couples strongly with the d_{xy} orbital but not with the d_{yz} and d_{zx} orbitals. It is also this orbital that is primarily responsible for the Van Hove singularity slightly above E_F at Brillouin zone boundary (20, 21). Most importantly it is the d_{xy} orbital that is primarily responsible to FM spin fluctuations (6, 9, 22). However, the d_{yz} and d_{zx} orbitals, which do not couple to the
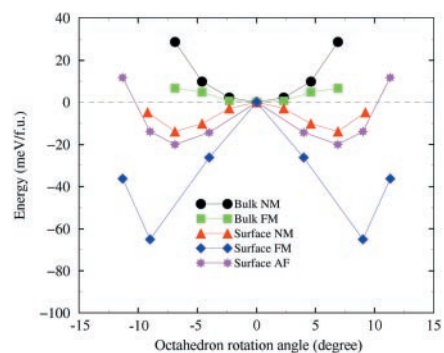
Fig. 3. Calculated total energy per f.u. versus octahedron rotation angle. Both FM and nonmagnetic (NM) cases are displayed for bulk and surface, respectively. The surface AF state corresponds to a state with planar $\mathbf{Q} = (\pi/a, \pi/a)$. The curves are shifted to make energies of nonrotated structures equal to zero. The surface FM state is lower in energy by about 5 meV compared with other magnetic states for the nonrotated structures.

Σ_3 bulk-phonon mode, contribute to the two other sheets of the Fermi surface, and produce the incommensurate spin fluctuations due to dynamical Fermi surface nesting (6). The spin degrees of freedom in the d_{xy} and the $d_{yz,zx}$ orbitals behave more or less independently (7).

In general, a rotation of the octahedra reduces the effective lateral d-d hopping and causes band narrowing, which can lead to a

Mott-insulating AF phase (*23*). However, at the surface of Sr$_2$RuO$_4$, our calculations show that band narrowing increases the density of states at the Fermi energy, which will stabilize the FM order. As expected, the bandwidth of the d_{xy} orbital becomes narrower as the octhedra rotates, which for the nonmagnetic case pulls the VHS slightly below the Fermi energy. The high density of states at the Fermi energy enhances FM spin fluctuations and, in this case, leads to a FM ground state at the surface. This observation at the surface of Sr$_2$RuO$_4$ opens up many exciting prospects relevant to the bulk and surface properties of these layered transition metal oxides. One exciting example is the coexistence of FM order and superconductivity (*24*, *25*).

References and Notes
1. Y. Maeno *et al.*, *Nature* **372**, 532 (1994).
2. G. M. Luke *et al.*, *Nature* **394**, 558 (1998); T. M. Riseman *et al.*, *Nature* **396**, 242 (1998); K. Ishida *et al.*, *Nature* **396**, 658 (1998).
3. T. M. Rice and M. Sigrist, *J. Phys. Condens. Matter* **7**, L643 (1995).
4. M. Braden *et al.*, *Physica C* **273**, 248 (1997).
5. M. Braden *et al.*, *Phys. Rev. B* **57**, 1236 (1998).
6. T. Imai *et al.*, *Phys. Rev. Lett.* **81**, 3006 (1998).
7. H. Mukuda *et al.*, *J. Phys. Soc. Jpn.* **67**, 3954 (1998); *Phys. Rev. B* **60**, 12279 (1999).
8. I. I. Mazin and D. J. Singh, *Phys. Rev. Lett.* **79**, 733 (1997); L. Tewordt, *Phys. Rev. Lett.* **83**, 1007 (1999).
9. I. I. Mazin and D. J. Singh, *Phys. Rev. Lett.* **82**, 4324 (1999).
10. Y. Sidis *et al.*, *Phys. Rev. Lett.* **83**, 3320 (1999).
11. The samples were glued with silver epoxy on a holder, and a metal post was glued on top of the sample. After introduction into an ultrahigh vacuum ($<10^{-10}$ mbar), they were cleaved at room temperature by breaking off the post.
12. Samples cleaved at $T < 4$ K also exhibit ($\sqrt{2} \times \sqrt{2}$)R45° reconstruction [E. W. Hudson *et al.*, *Bull. Am. Phys. Soc.* **44**, 1369 (1999)].
13. We thank P. Dai and H. Kawano for supplying the second sample.
14. D. Vanderbilt, *Phys. Rev. B* **41**, 7892 (1990).
15. P. K. De Boer and R. A. de Groot, *Phys. Rev. B* **59**, 9894 (1999).
16. Theory predicts that the ground state of the surface is FM. A crucial question is what is the magnetic transition temperature? Unfortunately, the precision of the LEED structural determination cannot be used to determine the difference between the 6.5° rotation for a nonmagnetic surface and 9° rotation for a magnetic surface predicted by theory. A theoretical determination of the transition temperature would require a calculation of the excitation states of the system, which is beyond our ability.
17. T. Yokoya *et al.*, *Phys. Rev. Lett.* **76**, 3009 (1996).
18. D. H. Lu *et al.*, *Phys. Rev. Lett.* **76**, 4845 (1996).
19. A. V. Puchkov *et al.*, *Phys. Rev. B* **58**, R13322 (1998).
20. A. P. Mackenzie *et al.*, *Phys. Rev. Lett.* **76**, 3786 (1996).
21. T. Oguchi, *Phys. Rev. B* **51**, 1385 (1995); D. J. Singh, *Phys. Rev. B* **52**, 1358 (1995).
22. D. F. Agterberg, T. M. Rice, M. Sigrist, *Phys. Rev. Lett.* **78**, 3374 (1997).
23. N. F. Mott, *Metal-Insulator Transitions* (Taylor & Francis, New York, ed. 2, 1990).
24. W. E. Pickett *et al.*, *Phys. Rev. Lett.* **83**, 3713 (1999).
25. C. Bernhard *et al.*, *Phys. Rev. B* **59**, 14099 (1999).
26. We acknowledge the use of the Barbieri/Van Hove Symmetrized Automated Tensor LEED package, available from M. A. Van Hove. R.M. gratefully acknowledges a Feodor Lynen fellowship of the Alexander von Humboldt foundation. Supported by JRCAT, NSF, and DOE.

31 April 2000; accepted 7 June 2000

Radiation Tolerance of Complex Oxides

K. E. Sickafus,[1]* L. Minervini,[2] R. W. Grimes,[2] J. A. Valdez,[1] M. Ishimaru,[3] F. Li,[1] K. J. McClellan,[1] T. Hartmann[1]

The radiation performance of a variety of complex oxides is predicted on the basis of a material's propensity to accommodate lattice point defects. The calculations indicate that a particular class of oxides possessing the fluorite crystal structure should accept radiation-induced defects into their lattices far more readily than a structurally similar class of oxides based on the pyrochlore crystal structure. Preliminary radiation damage experiments substantiate the prediction that fluorites are inherently more radiation resistant than pyrochlores. These results may permit the chemical durability and radiation tolerance of potential hosts for actinides and radioactive wastes to be tailored.

One of the principal factors complicating the selection of materials for nuclear waste storage is the susceptibility of waste forms to detrimental radiation damage effects. Several crystalline ceramics, such as zircon (ZrSiO$_4$) and the orthophosphate monazite (LnPO$_4$; Ln = La, Ce, Nd, Gd, and others in the lanthanide series), exhibit both high chemical durability and solubility for actinides and other radionuclides, and are therefore attractive candidates for nuclear-waste host materials (*1*, *2*). However, among the chemically stable host phases proposed for waste storage, there is a paucity of materials for which long-term stability can be anticipated. This is because radioactive constituents in high-level waste (HLW) can decay to produce numerous atomic defects. Most materials are destabilized by such defects, and if defect accumulation is allowed to proceed unchecked, crystalline oxides ultimately succumb to an amorphization transformation, often accompanied by significant volume changes (*3*) and concomitant microcracking (*4*).

The technical challenge for HLW storage has therefore been to identify materials for which deleterious radiation effects are averted even at very high self-radiation exposures. The principal consequence of a displacive radiation environment is an elevated population in the lattice of Frenkel pairs (each pair consisting of an atomic interstitial and a lattice vacancy). Subsequent damage evolution hinges on two important factors. First is the degree to which lattice stability is affected by the accumulation of point defects. This factor influences a materials propensity to amorphize under irradiation. The second factor concerns the ultimate fate of irradiation-induced point defects. Interstitials and vacancies can migrate and annihilate harmlessly by interstitial-vacancy (*i-v*) recombination (the reverse of a Frenkel reaction), or they can cluster with other interstitials and vacancies to precipitate interstitial dislocation loops and voids. A material in which clustering occurs with ease will likely be susceptible to void swelling.

Many simple oxides such as magnesia (MgO) and alumina (Al$_2$O$_3$) are susceptible to void swelling (*5*). On the other hand, and perhaps surprisingly, a compound made from an equimolar mixture of MgO and Al$_2$O$_3$ (best known as the mineral spinel, MgAl$_2$O$_4$) is highly resistant to void swelling under neutron irradiation (*5*). The radiation-resistant behavior of spinel, which is exceptional for a ceramic, is most likely due to the following factors: (i) Complex chemistry causes the critical size of a dislocation loop nucleus to become unusually large (*6*). This necessarily suppresses loop nucleation. (ii) Complex structure generates constraints that prohibit dislocation loops from easily unfaulting (*7*). Faulted interstitial loops remain poor sinks (compared to unfaulted loops) for interstitial absorption. (iii) Some materials like spinel readily accommodate disordering defects within their structures. In fact, the cation sublattices in spinel can be completely disordered by high-fluence neutron irradiation (*8*). For all of these reasons, harmless *i-v* recombination (including cation antisite formation, i.e., swapping the position of one Mg cation with one Al cation) in spinel is a highly efficient point defect annihilation mechanism, and void swelling is negligible.

To test the generality of these attributes for radiation tolerance, we recently initiated an investigation into the radiation damage behavior of an extensive class of complex oxides known as pyrochlores. Oxide pyrochlores are typically ternary compounds of the general formula A$_2$B$_2$O$_7$ (where A and B are metallic cations). The simplest pyrochlore

[1]Division of Materials Science and Technology, MS-G755, Los Alamos National Laboratory, Los Alamos, NM 87545, USA. [2]Department of Materials, Imperial College, Prince Consort Road, London SW7 2BP, UK. [3]The Institute of Scientific and Industrial Research, Osaka University, Mihogaoka, Ibaraki, Osaka 567-0047, Japan.

*To whom correspondence should be addressed. E-mail: kurt@lanl.gov